Available online at www.sciencedirect.com

SciVerse ScienceDirect

Procedia Computer Science 9 (2012) 1004 – 1013

Procedia Computer Science

International Conference on Computational Science, ICCS 2012

Fourth order transport model on Yin-Yang grid by multi-moment constrained finite volume scheme

Xingliang Li[a], Xueshun Shen[a], Xindong Peng[b], Feng Xiao[c], Zhaorong Zhuang[a], Chungang Chen[d,1,*]

[a]*Center of Numerical Weather Prediction, China Meteorological Administration, Beijing, 100081, China*
[b]*State Key Laboratory of Severe Weather, Chinese Academy of Meteorological Sciences, Beijing, 100081, China*
[c]*Department of Energy Sciences, Tokyo Institute of Technology, Yokohama, 226-8502, Japan*
[d]*School of Human Settlement and Civil Engineering, Xi'an Jiaotong University, Xi'an, 710049, China*

Abstract

A fourth order transport model is proposed for global computation with the application of multi-moment constrained finite volume (MCV) scheme and Yin-Yang overset grid. Using multi-moment concept, local degrees of freedom (DOFs) are point-wisely defined within each mesh element to build a cubic spatial reconstruction. The updating formulations for local DOFs are derived by adopting multi moments as constraint conditions, including volume-integrated average (VIA), point value (PV) and first order derivative value (DV). Using Yin-Yang grid eliminates the polar singularities and results in a quasi-uniform mesh over the whole globe. Each component of Yin-Yang grid is a part of the LAT-LON grid, an orthogonal structured grid, where the MCV formulations designed for Cartesian grid can be applied straightforwardly to develop the high order numerical schemes. Proposed MCV model is checked by widely used benchmark tests. The numerical results show that the present model has fourth order accuracy and is competitive to most existing ones.

Keywords:
Transport model, Yin-Yang grid, Finite volume scheme, High order scheme

1. Introduction

Since 1990s, high-resolution GCM (General Circulation Model) simulations have become technically possible with the rapid development of computer hardware. To develop the high performance global models for such kind of simulations, researchers began to pay more attentions to computational meshes with global quasi-uniform grid spacing. So far, the representative advanced spherical meshes include cubed-sphere grid [1], icosahedral-triangular grid, icosahedral-hexagonal grid [2, 3] and Yin-Yang grid [4].

Cubed-sphere grid is constructed by projecting an inscribed cube onto the sphere. It covers the whole global with six identical patches, where the curvilinear coordinates are constructed. Cubed-sphere grid eliminates the equation

* *Email address:* cgchen@mail.xjtu.edu.cn (Chungang Chen)
[1]Corresponding author address: School of Human Settlement and Civil Engineering, Xi'an Jiaotong University, No. 28, Xianning West Road, Xi'an, 710049, China.

doi:10.1016/j.procs.2012.04.108

singularities and circumvents the convergence of meridian lines near two poles. Its major disadvantage compared with LAT-LON grid is that the coordinate system might be non-orthogonal and then results in more complicated numerical formulations. Furthermore, the discontinuous local coordinates along patches boundaries often introduce extra numerical errors. Conformal cubic grid was proposed in [5] to obtain the continuous local coordinates at patch boundaries, but at the cost of losing analytical transformation relations. Global quasi-uniform meshes could also be constructed by projecting the icosahedron onto the sphere and the resulted grids possess considerably uniform grid spacing. Two kinds of grids, i.e. icosahedral-triangular grid and icosahedral-hexagonal grid, have been becoming popular in GCM community recently. However, these spherical grids are unstructured in nature. The numerical models on these unstructured meshes require numerical techniques which are very different from those developed for the structured grids and are much more complicated. Generally, the numerical models running on unstructured grids are usually more computational expensive and more challenging for parallel implementations. Meanwhile, it is usually not a trivial work to develop high order schemes (more than second order accuracy) over an unstructured grid.

Yin-Yang grid (shown in Fig.1) was recently introduced by [4]. Being an overset grid, Yin-Yang grid is constructed by combining two perpendicularly oriented LAT-LON grid components of low latitude part, which is quasi-uniform and free from the polar singularity. Since each component of Yin-Yang is part of the conventional LAT-LON grid, it is very attractive for GCM modelers. It provides a convenient platform to directly transplant the existing numerical models developed on the latitude-longitude grid. Being an overset grid, Yin-Yang grid needs to communicate data in the overlapping area between Yin and Yang components which does not automatically guarantee the total mass conservation over the sphere, though conservative schemes are adopted within two component grids. A transport model was proposed in [6] to assure the global conservation on Yin-Yang grid by adjusting the flux computation for the cells in the overlapping area based on a piecewise constant reconstruction. The scheme adopted in [7] for high order mass integration over spherical polygons might be a potential choice for higher order implementations.

We have shown in our previous work [8] that numerical errors, including those in in mass conservation, can be remarkably reduced by implementing high order local reconstructions using multi-moments. In this paper, we concentrate on developing a fourth order accurate atmospheric transport model for the Yin-Yang grid by using high order MCV scheme. The numerical results show that the resulting model assures adequate accuracy for medium range weather prediction or short range climate simulation.

Multi moment constrained finite volume (MCV) scheme was proposed in [9]. This scheme introduced a novel numerical framework for developing the arbitrary high order schemes. Instead of using multi moments as model variables directly, degrees of freedom (DOFs) for high order reconstruction are locally defined as point-wise values at specified points within each cell. Multi moments (constraints) including volume-integrated average (VIA), point values (PVs) and derivatives of different orders (DVs) are adopted to provide the spatial discretization formulations for local DOFs. Third to sixth order MCV schemes for system of conservation laws have been constructed on Cartesian grid in [9]. The MCV schemes are computational efficient due to concise evolution equations for different moments. Furthermore, MCV schemes allows larger CFL stability conditions compared with discontinuous Galerkin schemes and spectral volume/difference schemes of same order. As we know, smooth but considerably complex structures are main characteristic of geophysical flows. To accurately simulate such phenomena, high order scheme are preferred. We have developed a global shallow water model based on Yin-Yang grid in [8] using conservative semi-Lagrangian scheme. Though semi-Lagrangian schemes are wildly used in GCMs, it is not easy to treat the integration of source terms along the trajectory with uniform high order accuracy. For general systems of conservation laws, we prefer to adopt the high order schemes developed under Eulerian framework. In this paper, we develop a global transport model by extending the fourth order MCV scheme to spherical geometry with the application to Yin-Yang grid.

The remaining part of this paper is organized as follows. We describe the fourth order MCV formulations for solving transport equation on Yin-yang grid in section 2. Section 3 includes the numerical results of wildly used benchmark tests by proposed model and the comparisons with other representative global transport models for verification. At last, a short conclusion is given in section 4.

2. Spherical transport model on the Yin-Yang grid

2.1. Yin-Yang overset grid

The Yin-Yang overset grid consists of two components. Each one is nothing but the lower latitude part of the conventional LAT-LON grid. As a result, the grid spacing of the Yin-Yang grid is quite uniform. To cover the whole

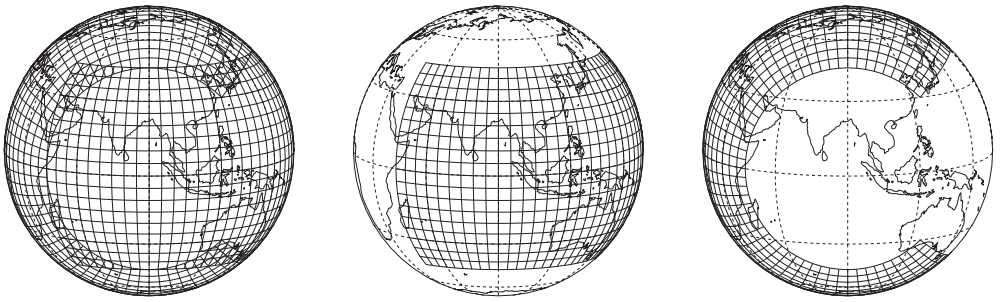

Figure 1: Schematic diagram of the Yin-Yang grid (left), which consists of two notched LAT-LON grids, i.e. Yang grid (middle) and Yin grid (right), perpendicularly oriented to each other. Each component grid covers a domain of longitudinal 270 degrees and latitudinal 90 degrees.

global, the computational domain (Yin- or Yang grid) is at least defined to be from 45°S to 45°N in latitudinal direction and from 45°E to 315°E in longitudinal direction. Two components of Yin-Yang grid are normal to each other, the transformation laws between Yin coordinate (λ', φ') and Yang coordinate (λ, φ) is easily written as

$$\begin{cases} \cos\varphi\cos\lambda &= -\cos\varphi'\cos\lambda' \\ \cos\varphi\sin\lambda &= \sin\varphi' \\ \sin\varphi &= \cos\varphi'\sin\lambda' \end{cases}. \tag{1}$$

Bearing in mind that the Yin and Yang components are identical, the same numerical formulations can be independently used on Yin or Yang component if the enough ghost cells are interpolated from the adjacent component. The locations of ghost cells are calculated and stored at the beginning of the computation. MCV scheme is constructed based on single-cell reconstructions. As a result, only one-layer ghost cells are required to exchange the information over Yin and Yang components. Using local high-order reconstructions, interpolation stencil used for evaluating the ghost cell is within one computational element. Such compact stencil is useful not only for improving computational efficiency, but also suppressing the extra numerical errors generated by nonconforming connections between Yin and Yang components. For sake of brevity, we specify our discussions in the following sections only to the Yang grid.

2.2. Fourth order MCV transport model on Yin-Yang grid

In this subsection, we describe the numerical formulations of fourth order MCV model for global transport computation on Yin-Yang grid.

Two dimensional spherical transport equation is written on the LAT-LON grid in conservative form as

$$\partial_t\psi + \partial_\lambda e + \partial_\varphi f = 0, \tag{2}$$

where $\psi = \sqrt{G}\phi$, ϕ is the transported field, $\sqrt{G} = a^2\cos\varphi$ is the Jacobian of transformation, a is the Earth radius, λ and φ denote the longitude and latitude direction on sphere, flux vector $\mathbf{f} = (e, f) = (\psi\tilde{u}, \psi\tilde{v})$, and $\tilde{\mathbf{v}} = (\tilde{u}, \tilde{v}) = (\frac{u}{a\cos\varphi}, \frac{v}{a})$ is the angular velocity on LAT-LON grid.

Third order spatial reconstruction over each control volume is required to construct fourth order MCV model. As a result, 16 local DOFs should be defined within each control volume for single-cell reconstruction. As shown in computational space in Fig.2, 16 local DOFs (ϕ_{ijmn} where the local DOF indices m (1 to 4) and n (1 to 4) indicate the positions within the control volume of the indices ij) are equidistantly arranged in logical rectangular control volume C_{ij}. The discretization formulations for these local DOFs through constraint conditions provided by multi moments were developed in [9] as so-called multi-moment finite volume (MCV) scheme. We hereafter describe the implementation of fourth order MCV scheme for global transport computation on Yin-Yang overset grid.

To construct a high order model, derivatives of flux vectors (second and third terms of Eq. (2)) are firstly computed through MCV scheme to obtain the semi-discrete equations. Then the time integration is accomplished by using fourth order Runge-Kutta scheme.

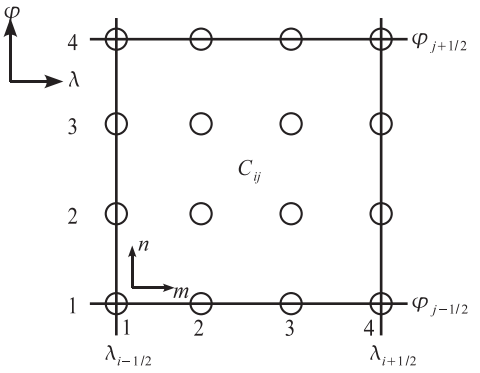

Figure 2: The equidistant local DOFs are defined within the control volume $C_{ij} = [\lambda_{i-1/2}, \lambda_{i+1/2}]\times[\varphi_{j-1/2}, \varphi_{j+1/2}]$ where 16 local DOFs are denoted as the blank circles for the fourth-order MCV model. There are four rows (grid lines) in λ-direction and four columns (grid lines) in φ-direction within the control volume, respectively.

On structured grid, MCV scheme are efficiently implemented by using one dimensional formulations in different directions one by one along grid lines. Without losing generality, we consider the determination of the derivative of flux component e with respect to λ. Similar procedure by exchanging e with f and λ with φ can be used along grid lines in φ-direction.

Considering the local DOFs defined along nth (n=1 to 4) row within control volume C_{ij} (Fig.2), we describe the numerical procedure to calculate the derivative of flux e with respect to λ. To build an even order MCV scheme, constraints are defined both at cell's interfaces and inside the cell. For fourth order scheme, constraints are adopted as

- Point values of flux component e at two endpoints of control volume, i.e. e_{ij1n} and e_{ij4n}, which are used in the flux-form formulation for the Line-Integrated Average (LIA) moment over the line segment in λ direction;
- First order derivative values of flux component e at two ends of control volume, i.e. $(\partial_\lambda e)_{ij1n}$ and $(\partial_\lambda e)_{ij4n}$, which are used to update the Point Value (PV) moment;
- Second order derivative value of flux component e at the center of control volume, i.e. $\left(\partial^2_\lambda e\right)_{ijCn}$, which provides another constraint in terms of the Derivative (DV) moment.

The following relationship connects the constraints and the point-wise derivatives of the flux components e with respect to λ at specified points from P_{ij1n} to P_{ij4n} which are directly then to update the unknowns,

$$\begin{bmatrix} (\partial_\lambda e)_{ij1n} \\ (\partial_\lambda e)_{ij2n} \\ (\partial_\lambda e)_{ij3n} \\ (\partial_\lambda e)_{ij4n} \end{bmatrix} = \mathbf{M} \begin{bmatrix} e_{ij1n} \\ e_{ij4n} \\ (\partial_\lambda e)_{ij1n} \\ (\partial_\lambda e)_{ij4n} \\ \left(\partial^2_\lambda e\right)_{ijCn} \end{bmatrix}, \tag{3}$$

where

$$\mathbf{M} = \begin{bmatrix} 0 & 0 & 1 & 0 & 0 \\ -\frac{4}{3\Delta\lambda} & \frac{4}{3\Delta\lambda} & -\frac{4}{27} & -\frac{5}{27} & -\frac{4\Delta\lambda}{27} \\ -\frac{4}{3\Delta\lambda} & \frac{4}{3\Delta\lambda} & -\frac{4}{27} & -\frac{5}{27} & \frac{4\Delta\lambda}{27} \\ 0 & 0 & 0 & 1 & 0 \end{bmatrix}. \tag{4}$$

The discretization formulations for different constraints (moments) are derived by the following steps.

- One dimensional cubic Lagrangian interpolation function is constructed for advected field ψ using the point values at points P_{ij1n} to P_{ij4n} as

$$\Psi(\lambda)_{ijn} = \sum_{m=1}^{4} \left(\mathcal{P}_m \psi_{ijmn}\right), \tag{5}$$

where basis function is

$$\mathcal{P}_m = \prod_{p=1,p\neq m}^{4} \frac{\left(\lambda - \lambda_p\right)}{\left(\lambda_m - \lambda_p\right)}. \tag{6}$$

- Numerical fluxes at cell interfaces are determined directly from the point values of the transported field as

$$e_{ij1n} = \tilde{u}_{ij1n}\psi_{ij1n} \text{ and } e_{ij4n} = \tilde{u}_{ij4n}\psi_{ij4n}. \tag{7}$$

- Derivatives of flux is determined by solving general Riemann problem (GPR), also known as the derivative Riemann Problem (DRP), at cell interfaces. For example, at left interface of cell C_{ij}, it is computed as

$$(\partial_\lambda e)_{ij1n} = \frac{1}{2}\left[(\partial_\lambda E_l)_{ij1n} + (\partial_\lambda E_r)_{ij1n}\right] + \frac{\left|\tilde{u}_{ij1n}\right|}{2}\left[(\partial_\lambda \Psi_l)_{ij1n} - (\partial_\lambda \Psi_r)_{ij1n}\right], \tag{8}$$

where E and Ψ are the spatial reconstructions of flux component e and variable $\psi = \sqrt{G}\phi$, subscript l denotes nth row of control volume C_{i-1j} and r denotes the nth row of C_{ij}.

- The second order derivative of flux component e with respect to λ is computed by following procedure:

(1) A fourth-order reconstruction polynomial $\mathcal{E}$ for flux component e along the nth row of control volume C_{ij} is obtained with the constraints as

$$\begin{cases} \mathcal{E}\left(\lambda_{i-\frac{1}{2}}\right) &= e_{ij1n} \\ \mathcal{E}\left(\lambda_{i+\frac{1}{2}}\right) &= e_{ij4n} \\ \partial_\lambda \mathcal{E}\left(\lambda_{i-\frac{1}{2}}\right) &= (\partial_\lambda e)_{ij1n}, \\ \partial_\lambda \mathcal{E}\left(\lambda_{i+\frac{1}{2}}\right) &= (\partial_\lambda e)_{ij4n} \\ \mathcal{E}\left(\lambda_i\right) &= E\left(\lambda_i\right) \end{cases} \tag{9}$$

(2) Then the second order derivative of flux component e with respect to λ at cell's center is computed as

$$(\partial_{\lambda\lambda} e)_{ijCn} = \partial_\lambda^2 \mathcal{E}\left(\lambda_i\right). \tag{10}$$

After accomplishing the spatial discretization, the ordinary differential equation

$$\partial_t \psi_{ijmn} = \mathcal{L}\left(\psi\right) \tag{11}$$

is solved by fourth order Runge-Kutta scheme from step k to step $k+1$ as

$$\begin{aligned} \psi^{(1)}_{ijmn} &= \psi^k_{ijmn} + \frac{1}{2}\Delta t \mathcal{L}(\psi^k_{ijmn}) \\ \psi^{(2)}_{ijmn} &= \psi^k_{ijmn} + \frac{1}{2}\Delta t \mathcal{L}(\psi^{(1)}_{ijmn}) \\ \psi^{(3)}_{ijmn} &= \psi^k_{ijmn} + \Delta t \mathcal{L}(\psi^{(2)}_{ijmn}) \\ \psi^{n+1}_{ijmn} &= -\frac{1}{3}\psi^k_{ijmn} + \frac{1}{3}\psi^{(1)}_{ijmn} + \frac{2}{3}\psi^{(2)}_{ijmn} + \frac{1}{3}\psi^{(3)}_{ijmn}. \end{aligned} \tag{12}$$

3. Numerical tests

In this section, we present three widely used numerical examples for global transport to evaluate the numerical scheme. The convergence rate of the numerical scheme is examined by grid refinement tests for the spherical advection transport problem. The solid body transport test for advection equation proposed by [10] and another recently suggested moving-vortex test is utilized to examine the performance of the numerical scheme for practical applications. Normalized error measures l_1, l_2 and l_∞ on the Yin-Yang grid in details are defined in [8].

3.1. Accuracy test

A smooth initial distribution is specified for accuracy test as

$$\phi(\lambda, \varphi, 0) = \cos\varphi^2 \sin 2\lambda. \tag{13}$$

Solid rotations in different directions are tested with the velocity field as

$$\begin{cases} u &= u_0(\cos\varphi\cos\alpha + \sin\varphi\cos\lambda\sin\alpha) \\ v &= -u_0\sin\lambda\sin\varphi \end{cases}, \tag{14}$$

where the parameter α is the angle between the axis of the solid body rotation and the polar axis of the spherical coordinate system, and $u_0 = 2\pi a/(12\text{days})$

Normalized errors by present model on a series refining grids are given in Table 1, Table 2 and Table 3 for solid rotations in different directions. According to these results, the fourth order accuracy of present model are verified as expected.

Table 1: Convergence rate of solid rotation in east direction ($\alpha = 0$) on Yin-Yang grid.

Resolution	l_1		l_2		l_∞	
(step)	error	order	error	order	error	order
11.25° (480)	3.69e-4	-	3.69e-4	-	4.15e-4	-
5.625° (960)	2.14e-5	4.11	2.10e-5	4.14	2.15e-5	4.27
2.8125°(1920)	1.26e-6	4.09	1.24e-6	4.08	1.54e-6	3.80

Table 2: Same as Table 1, but in northeast direction ($\alpha = \frac{\pi}{4}$).

Resolution	l_1		l_2		l_∞	
(step)	error	order	error	order	error	order
11.25° (480)	4.97e-4	-	5.11e-4	-	7.71e-4	-
5.625° (960)	3.14e-5	3.98	3.21e-5	3.99	3.94e-5	4.29
2.8125°(1920)	1.94e-6	4.02	1.97e-6	4.03	2.42e-6	4.03

Table 3: Same as Table 1, but in north direction ($\alpha = \frac{\pi}{2}$).

Resolution	l_1		l_2		l_∞	
(step)	error	order	error	order	error	order
11.25° (480)	8.94e-4	-	1.02e-3	-	1.24e-3	-
5.625° (960)	5.10e-5	4.13	5.39e-5	4.24	5.71e-5	4.44
2.8125°(1920)	2.94e-6	4.12	3.05e-6	4.14	3.29e-6	4.12

3.2. Cosine bell advection

Advection of a cosine bell, as the first test of Williamson's benchmark test set [10], is wildly checked to evaluate global models. The cosine bell is initially specified as

$$\phi(\lambda, \varphi) = \begin{cases} 0.5[1 + \cos(\pi r/R)] & \text{if } r < R = a/3 \\ 0 & \text{otherwise} \end{cases} \tag{15}$$

where $r = a\arccos\left[\sin\varphi_0\sin\varphi + \cos\varphi_0\cos\varphi\cos(\lambda - \lambda_0)\right]$, and the center of the distribution is $\lambda_0 = \pi/2$ and $\varphi_0 = 0$. The driving wind field is the same as the accuracy test case. Grid spacing is 4° in this case study, which corresponds to a grid resolution of $\frac{4}{3}^\circ$ in terms of DOFs.

Fig.3 shows that the cosine bell returns to its initial position after one revolution (12 days). The numerical contour lines (dashed lines) are visually identical to the analytic solution (solid lines). The history of normalized errors are shown in Fig.4 where the fluctuation in the normalized errors is observed when the cosine bell moves across the overlapping region of the Yin-Yang grid. Table 4 indicates the normalized errors after one revolution of rotation. It is noted that the normalized errors along the polar direction are larger than the others in Table 4 because in this case the advection path has more overlapping regions.

Compared with other models developed on LAT-LON grid (SLICE [11]), our result is competitive along the polar direction. Althrough the smaller CFL number is used against the SLICE scheme, the present model is easy to treat the source terms with uniform high order accuracy and the polar problems are avoided by utilizing the quasi-uniform Yin-Yang grid.

Numerical results of fourth order MCV model are better than those results of third order conservative semi-Lagrangian model [8] with an equivalent spatial resolution, for example, the numerical tests under the 1.40625° resolution in [8]. In addition, those are obviously better than [12] with their resolution of 1° on the Yin-Yang grid.

The simulation results on the Yin-Yang grid are also competitive to other multi-moment fourth order global models on the icosahedral grid [13] and on the cubed sphere [14] using similar degree of freedoms.

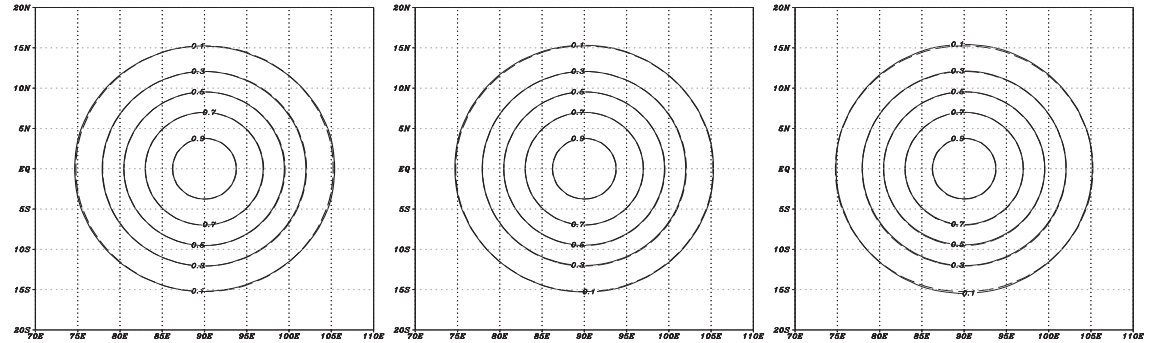

Figure 3: Numerical and exact solutions of cosine bell advection test at day 12 for different rotation directions with $\alpha = 0$(upper-left), $\alpha = \frac{\pi}{4}$(upper-right) and $\alpha = \frac{\pi}{2}$(bottom) on the grid with resolution of $\frac{4}{3}^\circ$. The solid line shows numerical result and dashed line shows exact solution. The contour interval is 0.2 from 0.1 to 0.9.

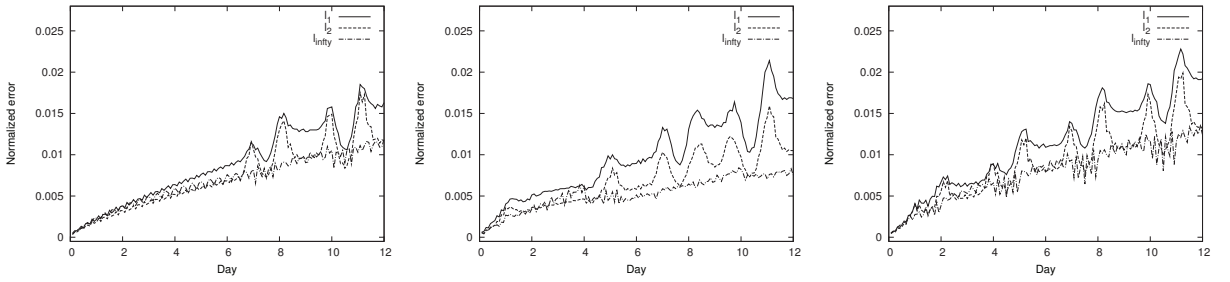

Figure 4: Normalized errors of solid-body test case with $\alpha = 0$(left), $\alpha = \frac{\pi}{4}$(middle) and $\alpha = \frac{\pi}{2}$(right) on the grid with DOFs resolution of $\frac{4}{3}^\circ$.

Table 4: Numerical results of cosine-bell advection test in different directions on Yin-Yang grid.

Direction (α)	l_1	l_2	l_∞
0	1.63e-2	1.17e-2	1.19e-2
$\frac{\pi}{4}$	1.68e-2	1.05e-2	7.54e-3
$\frac{\pi}{2}$	1.92e-2	1.31e-2	1.24e-2

3.3. Moving vortices

A more practical and challenging advection test is introduced in [15]. A complex velocity field is generated by superposing two vortical deformational flow fields whose vortex centers move along the trajectory of the solid rotation flow specified by Eq. (14). Detailed configuration of this test can be found in [15].

We run this test on grid with a resolution equivalent to 2.5° in terms of DOFs. Rotations of the vortex centers in three different directions, corresponding to $\alpha = 0$, $\alpha = \frac{\pi}{4}$ and $\alpha = \frac{\pi}{2}$, have been carried out. The time evolution of normalized errors along three different direction are depicted in Fig.5. It is observed that the errors are hardly influenced by the rotation direction.

As shown in [15], three methods including discontinuous Galerkin (DG) method, semi-Lagrangian method and finite volume (FV) methed are implemented for evaluating their performance in this moving vortex test . Compared with semi-Lagrangian method (see their Fig.5 for normalized errors), the normalized errors of the MCV scheme are obviously better in the case of the equivalent resolution with respect to the conventional LAT-LON sphere. The present model gives smaller errors in comparison with FV solution on the grid with same resolution (see their Fig. 7 for normalized errors). Although the DG method shows a little smaller normalized errors under the equivalent resolution, the MCV scheme allows larger CFL number for computational stability in the same order (see table 1 in [9]) and has a competitive computational efficiency since there is not any time-consuming volume integration involved. Contour plots of transport field ϕ and absolute errors are given in Fig.6 at different days. The location of moving vortex centers and phase of front of deforming vortices are accurately captured.

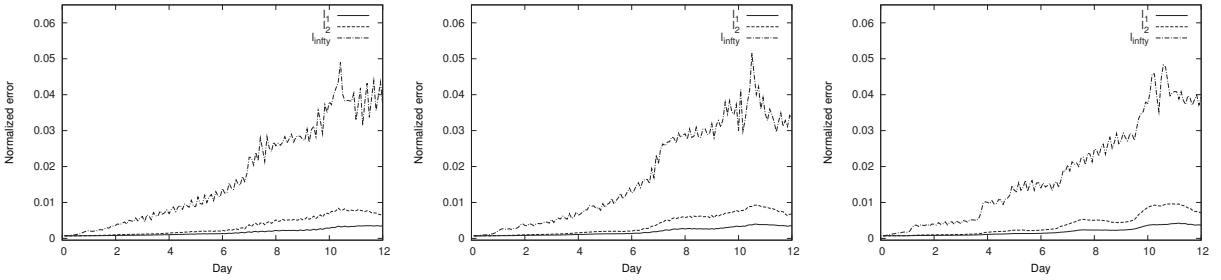

Figure 5: Normalized errors of moving vortex test case with $\alpha = 0$(left), $\alpha = \frac{\pi}{4}$(middle) and $\alpha = \frac{\pi}{2}$(right) on the grid with DOFs resolution of $2.5° \times 2.5°$.

4. Conclusion

A fourth order transport model on the spherical Yin-Yang grid is presented by using the multi-moment constrained finite volume (MCV) scheme. The MCV method uses local DOFs defined within single element at equally spaced points as the model variables. The evolution formulations for local DOFs are derived by adopting multi moments as constraint conditions, including volume integrated average (VIA), point value (PV) and spatial derivative value (DV) in our transport model. In the present model, the polar singularity and the convergence of meridians in the polar regions of conventional LAT-LON gird is completely avoided through utilizing the quasi-uniform Yin-Yang grid. The MCV scheme allows less restrictive CFL stability conditions in comparison with discontinuous Galerkin schemes and spectral volume schemes of same order. The widely used benchmark tests show that the present model has competitive high-order numerical accuracy and computational efficiency compared to most existing models.

References

[1] R. Sadourny, Conservative finite-difference approximations of the primitive equations on quasi-uniform spherical grids, Mon. Wea. Rev. 100 (2) (1972) 136–144.
[2] R. Sadourny, A. Arakawa, Y. Mintz, Integration of the nondivergent barotropic vorticity equation with an icosahedral-hexagonal grid for the sphere, Mon. Wea. Rev. 96 (6) (1968) 351–356.
[3] D. L. Williamson, Integration of the barotropic vorticity equation on a spherical geodesic grid, Tellus 20 (4) (1968) 642–653.
[4] A. Kageyama, T. Sato, The "Yin- Yang grid": An overset grid in spherical geometry, Geochem. Geophys. Geosyst. 5 (2004) Q09005.

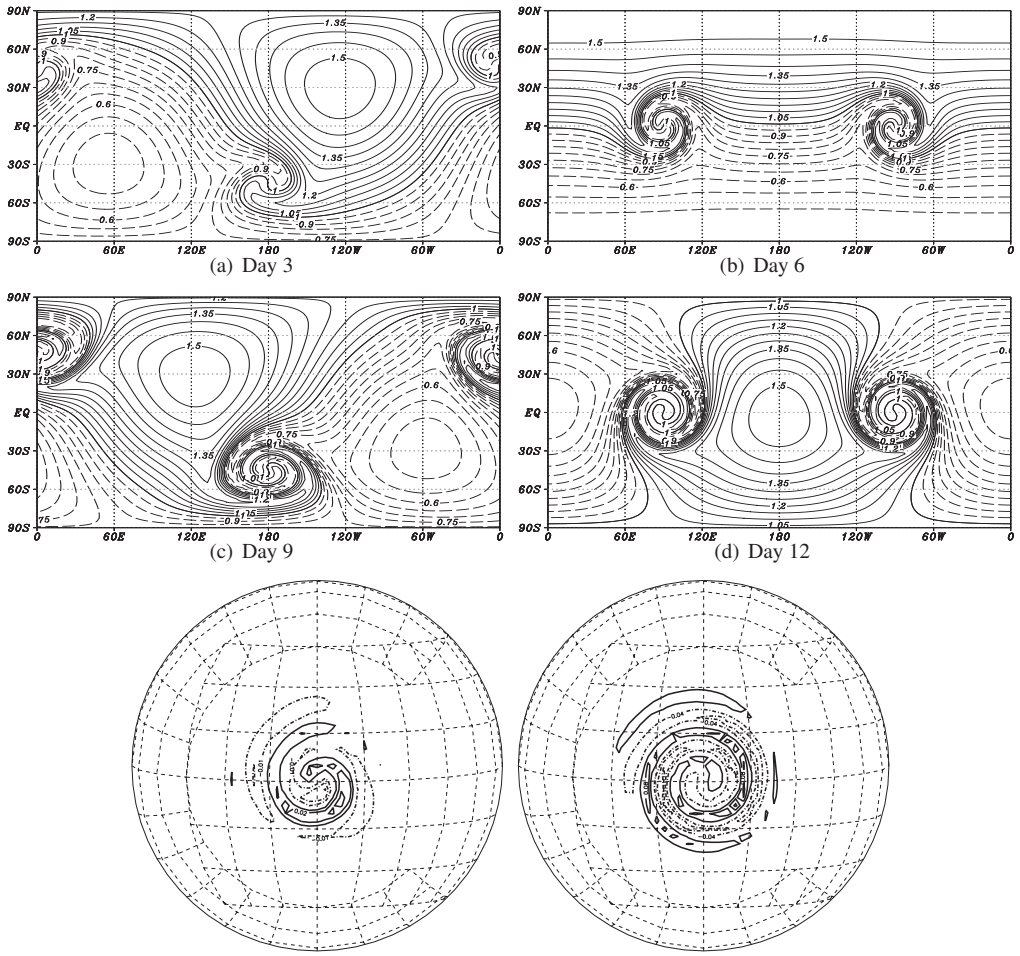

(a) Day 3 (b) Day 6

(c) Day 9 (d) Day 12

(e) the difference at Day 6 (f) the difference at Day 12

Figure 6: Numerical solution of the moving vortices with $\alpha = \frac{\pi}{4}$ at days 3, 6, 9, and 12 (after one full revolution) ((a)-(d)). The difference of numerical and exact solution at day 6, 12 ((e),(f)) and the contours are from -0.03 to 0.03 with 0.01 interval and from -0.12 to 0.12 with 0.04 interval, respectively. All snapshots are at the DOF resolution of $2.5^\circ \times 2.5^\circ$.

[5] M. Rancic, R. J. Purser, F. Mesinger, A global shallow-water model using an expanded spherical cube: gnomonic versus conformal coordinates, Q. J. R. Meteorol. Soc. 122 (532) (1996) 959–982.
[6] X. D. Peng, F. Xiao, K. Takahashi, Conservative constraint for a quasi-uniform overset grid on the sphere, Q. J. R. Meteorol. Soc. 132 (2006) 979–999.
[7] P. H. Lauritzen, R. D. Nair, P. A. Ullrich, A conservative semi-Lagrangian multi-tracer transport scheme (CSLAM) on the cubed-sphere grid, J. Comput. Phys. 229 (2010) 1401–1424.
[8] X. Li, D. Chen, X. Peng, K. Takahashi, F. Xiao, A multimoment finite-volume shallow-water model on the yin–yang overset spherical grid, Mon. Wea. Rev. 136 (8) (2008) 3066–3086.
[9] S. Ii, F. Xiao, High order multi-moment constrained finite volume High order multi-moment constrained finite volume method. Part I: Basic formulation, J. Comput. Phys. 228 (2009) 3668–3707.
[10] D. L. Williamson, J. B. Drake, J. J. Hack, R. Jakob, P. N. Swarztrauber, A standard test set for numerical approximations to the shallow water equations in spherical geometry, J. Comput. Phys. 102 (1) (1992) 211–224.
[11] M. Zerroukat, N. Wood, A. Staniforth, SLICE-S: A Semi-Lagrangian Inherently Conserving and Efficient scheme for transport problems on the Sphere, Q. J. R. Meteorol. Soc. 130 (2004) 2649–2664.
[12] Y. Baba, K. Takahashi, T. Sugimura, K. Goto, Dynamical core of an atmospheric general circulation model on a yin-yang grid, Mon. Wea. Rev. 138 (2010) 3988–4005.
[13] S. Ii, F. Xiao, Gloabl shallow water model using high order multi-moment constrained finite volume mehod and icosahedral grid, J. Comput. Phys. 229 (2010) 1774–1796.
[14] C. G. Chen, F. Xiao, Shallow water model on cubed-sphere by multi-moment finit volume scheme, J. Comput. Phys. 227 (2008) 5019?044.
[15] R. D. Nair, C. Jablonowski, Moving vortices on the sphere: a test case for horizontal advection problems, Mon. Wea. Rev. 136 (2008) 699–711.